CGL Technical Report, No. TP-2013-01, January 2013

Feature Fusion for Facial Landmark Detection
A Feature Descriptors Combination Approach

Panagiotis Perakis and Theoharis Theoharis
Computer Graphics Laboratory
Department of Informatics and Telecommunications
University of Athens, GREECE

Abstract Facial landmark detection is a crucial first step in facial analysis for biometrics and numerous other applications. However, it has proved to be a very challenging task due to the numerous sources of variation in 2D and 3D facial data. Although landmark detection based on descriptors of the 2D and 3D appearance of the face has been extensively studied, the fusion of such feature descriptors is a relatively under-studied issue. In this report, a novel generalized framework for combining facial feature descriptors is presented, and several feature fusion schemes are proposed and evaluated. The proposed framework maps each feature into a similarity score, combines the individual similarity scores into a resultant score, used to select the optimal solution for a queried landmark. The evaluation of the proposed fusion schemes for facial landmark detection clearly indicates that a quadratic distance to similarity mapping in conjunction with a root mean square rule for similarity fusion achieves the best performance in accuracy, efficiency, robustness and monotonicity.

Keywords Facial Landmarks, Feature Extraction, Feature Fusion, Landmark Detection

Version 1.0 Contact info: P. Perakis (p.perakis@di.uoa.gr.)

Computer Graphics Laboratory
Department of Informatics and Telecommunications
University of Athens
15784 Ilisia
GREECE
http://graphics.di.uoa.gr

Contents

1 Introduction

Facial landmark detection is a crucial first step in biometric applications, computer vision and computer graphics, and can be used for face registration, face recognition, facial expression recognition, facial shape analysis, segmentation and labeling of facial parts, facial region retrieval, partial face matching, facial mesh reconstruction, face relighting, face synthesis, face animation and motion capture. However, it has proved to be a very challenging task due to the numerous sources of variation in 2D and 3D facial data. These variations can be environment-based (illumination conditions and occlusions), subject-based (pose and expression variations) and acquisition-based (image scale, distortion, noise, spikes and holes). Both 2D and 3D facial landmark detection suffers from occlusion and expression variations. In addition, 2D facial landmark detection suffers from pose and illumination variations.

2D and 3D facial landmark detection is based on local descriptors of the 2D (intensity/color) or 3D (mesh/range) appearance of the face or of integral or differential transformations of it. Since a landmark detector has to possess the properties of repeatability and distinctiveness, local facial feature descriptors must be:
i) *robust*, to variations of facial data.
ii) *discriminative*, to distinguish between different anatomical landmarks.
iii) *descriptive*, to avoid similarity with outliers.
iv) *general*, to represent each landmark equally well on all "seen" faces.
v) *predictive*, to represent landmarks equally well on "unseen" faces.

To fulfill the above properties and constrain the detection process, landmark detectors use trained landmark classifiers or 2D/3D appearance landmark models/templates and 2D/3D geometry models for global topological consistency. 2D landmark detectors use view-based 2D geometry and appearance models or 3D geometry models. 3D landmark detectors use solely 3D geometry and 3D appearance models. Fused 2D/3D landmark detection methods use 3D geometry and 2D+3D appearance models. 2D and 3D landmark detection is based mostly on variations of the seminal work on Active Appearance Models of Cootes *et al.* [3, 5, 4, 6]. Fused 2D/3D landmark detection is presented in Boehnen & Russ [1], Jahanbin *et al.* [10], Lu & Jain [18], Passalis *et al.* [19] and Perakis *et al.* [20].

Although many 2D/3D descriptors of facial features are used in the literature, a crucial issue has not been answered yet. How can these facial features be fused together in order to exploit their individual strengths and create a robust and accurate landmark detector?

Different feature descriptors can have complementary strengths and weaknesses, so combining them can increase system *accuracy*, *efficiency* and *robustness*, featuring *monotonicity*. Accuracy can be increased by exploiting data content from multiple sources (3D/2D) or the strengths of different data descriptors. In addition, using multiple descriptors can improve efficiency by limiting the landmarks' likelihood area. Finally, fusion can increase system robustness by limiting deficiencies inherent in using a single descriptor. For example a corner/edge detector is very sensitive in illumination variations, but the shape index is not. Thus, using multiple descriptors is a form of uncertainty reduction, since one descriptor may pick up what the other misses.

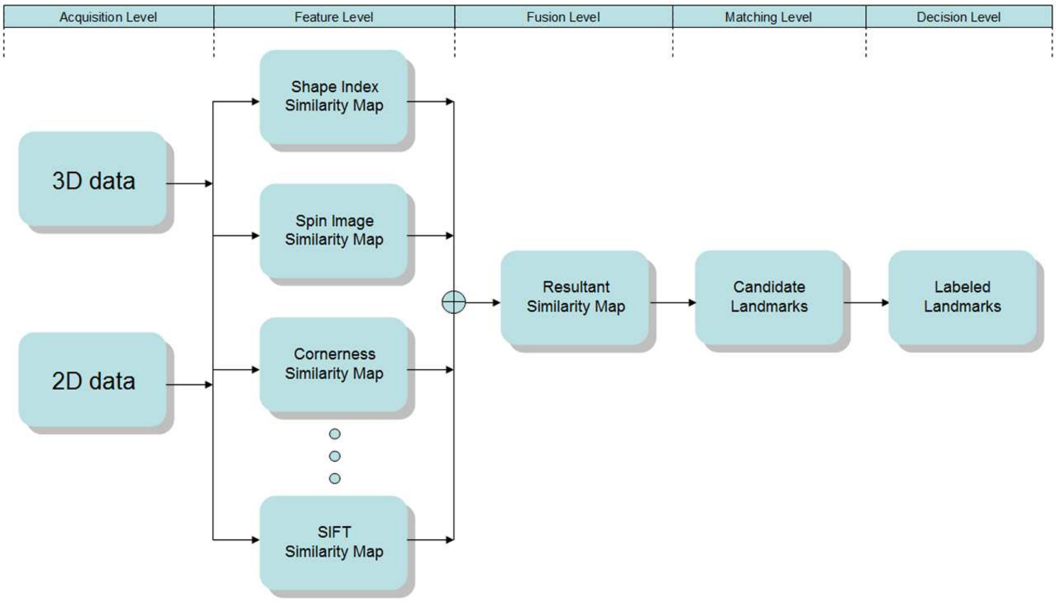

Figure 1: Pipeline of feature fusion procedure for landmark detection.

A landmark detector, has four important levels (Fig. 6). At the *acquisition level* a sensor acquires the facial data. At the *feature extraction level* the data are transformed into features that represent the landmark classes. At the *matching score level* the extracted features are compared with feature templates that represent each landmark class in order to detect candidate landmarks with an associated matching score. Finally, at the *decision level* the matching scores (or ranks) are used to select a candidate landmark as the optimal solution for the queried landmark class, and assign to it the label of the class. Landmark detection can thus be considered as a two-fold problem: (i) a search problem for candidates, and (ii) an identification problem for the labeling of candidates.

Fusion can be applied at the acquisition or feature extraction level (pre-classification fusion) and at the matching score or decision level (post-classification fusion) [12, 30]. Fusion at the matching score level can be viewed in two distinct ways. In the first, fusion is approached as a *classification* problem, while in the second, it is approached as a *combination* problem [12, 26]. In the classification approach, a composite feature vector (by weighted concatenation) is constructed using the values of the fused features, which is further classified by a composite classifier (e.g., Neural Network, K-NN, Decision Trees, SVM). In the combination approach, the matching scores of the fused features are combined to generate a single resultant feature score which is used for the final decision. The common characteristic of all combination techniques is that the individual feature classifiers are separately trained and the combination relies on simple fixed rules [26]. These rules are the *sum rule*, *product rule*, *max rule*, *min rule*, *median rule* and *majority voting* [15]. The various schemes for combining classifiers can be grouped into three main categories according to their architecture: (i) *parallel*, (ii) *cascading* (serial), and (iii) *hierarchical* (tree-like) [11].

An information fusion scheme should have the following fundamental properties,

as described in [2]:
Neutrality: The result of a fusion scheme should not be biased by the order in which the input features are processed.
Consistency: The result of a fusion scheme with one input feature should be the same as the result of this single feature.
Monotonicity: The result of a fusion scheme of two input features should have better quality than the individual results of each feature.
Significance: The result of a fusion scheme should preserve the significance of the input feature measured values.
Conviviality: Expresses the complexity/simplicity of a fusion scheme.
Transparency: Expresses the ability to explain and replicate the result of a fusion scheme (black-box effect).

For landmark detection, although the construction of a composite feature classifier might be a potential solution, the combination method can be more easily applied to features whose values can be mapped to images, is more transparent (having also the strength of visualization), and possesses all the other fundamental properties required by a fusion scheme.

This report provides a novel generalized framework of fusion methods and their application to landmark detection. The fusion scheme proposed acts after the "feature extraction level", transforms features to similarities and then combines them to generate a resultant feature similarity, which is considered as the matching score, and is used at the "matching level" for the detection of the queried landmarks (Fig. 6). The proposed approach of feature fusion is easily extendable by adding new feature-components in feature space and changing the resultant similarity appropriately. This approach works equally well for any feature extracted either from 3D or 2D facial data. The only prerequisite is the availability of a common (u,v) parameterization so that the 3D and 2D data can be combined at the "acquisition level".

The rest of this report is organized as follows: Section 2 describes related work in the field, Section 3 details the theoretical background of the proposed method, Section 4 presents its application to the detection of facial landmarks, Section 5 presents our results, and Section 6 summarizes our method.

2 Related Work

A number of studies showing the advantages of information fusion in pattern recognition and especially in multimodal biometrics have appeared in the literature.

Xu *et al.* [30] (1992) grouped different combining methods into categories and proposed methods for classifier fusion at different levels (measurement, rank and abstract). These combining methods were applied to recognizing handwritten numerals. They reported a significant improvement over the performance of individual classifiers.

Kittler *et al.* [15] (1998) have developed a theoretical framework for the combination approach to fusion at the matching score level of multimodal biometric applications. In their approach the matching scores of individual classifiers are interpreted as posterior probabilities and the resultant scores are the outcome of simple fixed fusion rules. They have experimented with several fusion rules (sum rule, product rule, max rule, min rule, median rule and majority voting) for face and voice biometrics and found that the sum rule outperformed the others. They also concluded that the sum rule is not significantly affected by the probability estimation errors and this explains its superiority.

Jain *et al.* [11] (2000) conducted experiments concerning the characteristics of combining twelve different classifiers using five different combination rules and six different feature sets generated from handwritten numerals (0-9). Reported results show that each case favors its own combining rule and that combining does not necessarily lead to improved peformance.

Ross and Jain [24] (2003) addressed the problem of information fusion in biometric verification systems by combining face, fingerprint and hand geometry modalities using sum, decision-tree and LDA based methods. They reported that the sum rule outperforms the others.

Jain *et al.* [12] (2005) presented a thorough classification of information fusion approaches in biometric systems. They also experimented with different normalization techniques (min-max, z-score, median, sigmoid, tanh and Parzen) and fusion rules (sum rule, max rule and min rule and weighted-sum rule) to combine score from different matchers in a multimodal biometric recognition system. They concluded that the tanh normalization is the most robust and efficient for a recognition system, and that weighted summation of the matching scores resulted in a significant improvement in recognition rates.

Ross and Govindarajan [23] (2005) have experimented with fusion at the feature level in 3 different scenarios: (i) fusion of PCA and LDA coefficients of face; (ii) fusion of LDA coefficients corresponding to the R,B,G channels of a face image; and (iii) fusion of face and hand modalities. They concluded that it is difficult to predict the best fusion strategy for a given scenario.

Snelick *et al.* [25] (2005) examined the performance of multimodal biometric authentication systems using fusion techniques over fingerprint and face modalities on a population approaching 1,000 individuals. They also introduced adaptive normalization techniques and weighted fusion rules. They concluded that multimodal fingerprint and face biometric systems can achieve better performance than unimodal systems.

Theoharis *et al.* [27] (2008) presented a multimodal biometric recognition system using the fusion of face and ear modalities. They reported that the fused multimodal system achieved better performance (99.7% rank-one recognition rate) than the unimodal systems. The high reported accuracy was attributed to the low correlation of the two modalities.

In landmark detection literature on the other hand the combination of landmark descriptors is an under-studied issue.

Lu and Jain [18] (2005) used the combination of shape index response derived from the range map (3D) and the cornerness response from the intensity map (2D) to determine the positions of the corners of the eyes and the mouth. They used a fusion scheme of a pixel-wise summation of the normalized shape index and cornerness response values, for the “resultant” feature values of mouth and eye corners.

Boehnen and Russ [1] (2005) used color images (2D) and range data (3D). A skin detection algorithm is applied using the YCbCr transformation of the initial RGB image. The face region that results from skin detection is refined by using z-erosion exploiting the range data. Thus, at first a face segmentation is applied; next, eye and mouth likelihood maps are calculated (using Cb and Cr values), to locate the corresponding landmarks. Thus this method is not a fusion method but merely a 2D/3D masking/filtering method.

Perakis *et al.* [20] (2009) and Passalis *et al.* [19] (2011) presented a 3D facial landmark detection system using the fusion of shape index and spin image feature descriptors. Their fusion system operated in a cascade (sequential) fashion so that the candidate landmarks extracted from the shape index transformation were classified and filtered out according to their similarity with precalculated spin image templates. They also used a product rule fusion of landmarks' geometric distance to a landmark model and spin image similarities at the decision level. They reported high landmark detection accuracy under large facial yaw rotations.

Jahanbin *et al.* [10] (2011) used Gabor jets to represent intensity (2D) and range (3D) data. Next, the jets of each pixel were compared (using the appropriate similarity measure) to a target bunch (describing the queried landmark) in order to create similarity maps for each modality and landmark class. Finally, intensity and and range similarity maps were combined into a "hybrid" similarity map ("resultant"). For the calculation of the "resultant" similarity map different approaches of fusion were examined such as taking the pixel-wise sum, product or maximum of the similarity scores. They concluded that summation is the most appropriate.

3 Feature Fusion for Landmark Detection

The features used for facial landmark detection have very different characteristics, but in general can be distinguished in scalar features (such as the Shape Index and Cornerness/Edge Response), and vector features (1D/2D histogram features, such as the SIFT descriptor and Spin Images). For each scalar feature we can statistically compute a corresponding target value, while for each vector feature we can compute a corresponding vector target (template), which represent a landmark in feature space. A distance metric for a scalar feature could be the absolute difference of its value from the corresponding target value, and for a vector feature the absolute difference of its similarity with the corresponding template from the maximum similarity (1.00).

Thus, instead of fusing features by weighted concatenation, the features are first transformed to similarities with a target value or template, and then each feature similarity can act as a component in a normalized feature similarity space (Fig. 2), which can be fused together to form a resultant feature similarity, using simple combination rules (such as sum, product, max, min, AND, OR and threshold masking). In this manner a dramatic dimensionality reduction is achieved since, instead of using multiple components for a vector feature, only the similarity with its template is used.

Each feature for a landmark class has a target value or template (t_f) that describes the landmark in its feature space. Furthermore, we can consider a cut-off

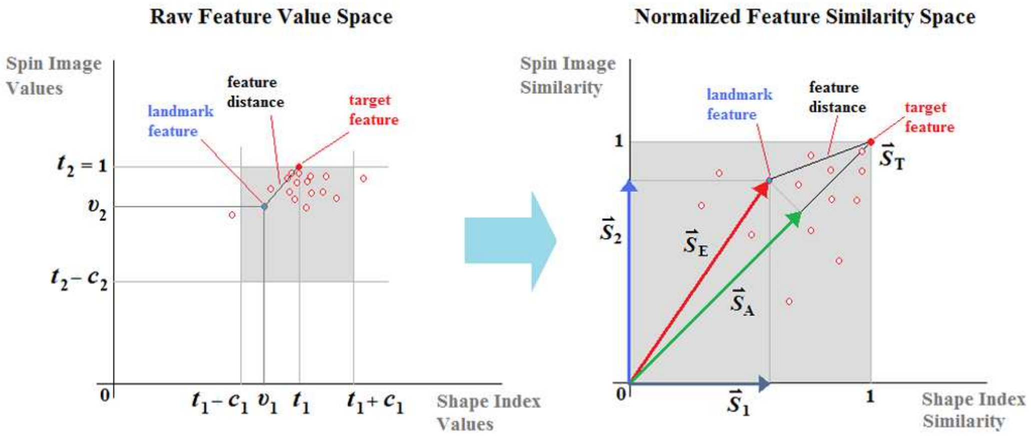

Figure 2: Example of the transformation from raw feature value space to normalized feature similarity space. Shape Index (v_1) and Spin Image (v_2) raw values are mapped onto Shape Index ($\mathbf{S_1}$) and Spin Image ($\mathbf{S_2}$) normalized similarity vectors. Note that the raw Spin Image values represent un-normalized similarity to the corresponding template.

value (c_f) for each feature to incorporate the notion of an outlier. Feature values out of the range $[t_f - c_f, t_f + c_f]$ can be filtered out, so that threshold masking is implemented. The cut-off value can also be considered as a scaling factor for the normalization of each feature's range (Fig. 2).

The target and cut-off values can be estimated by examining the probability distribution function (pdf) of feature values or set to specific values based on a priori knowledge. A good choice for the target value could be the mean of the pdf of feature values and for the cut-off value could be a multiple of standard deviation (std) (e.g., 3 × std as a first approximation), although the distribution of the values of every feature is not a Gaussian. Another choice for the target value could be the mode or the median of the pdf and the cut-off value could be determined so that a certain proportion of feature values (e.g., 99%) are within the range $[t_f - c_f, t_f + c_f]$.

For a good normalization scheme, the estimates of target (location), cut-off (scale) parameters and of the normalization function must be robust and efficient. In addition, a properly designed fusion method exploits information from each descriptor without degrading performance below that of the most accurate descriptor (monotonicity). This is the major challenge of adopting a fusion scheme.

3.1 Feature similarity mapping

Given a feature value v_f, a target value t_f and a cut-off value c_f for each feature descriptor f, we introduce a *normalized distance measure* to target D_f for each of the N feature descriptors of each landmark point:

$$D_f = \begin{cases} \dfrac{|v_f - t_f|}{c_f} & \text{if } |v_f - t_f| \leq c_f \\ 1 & \text{otherwise} \end{cases} \tag{1}$$

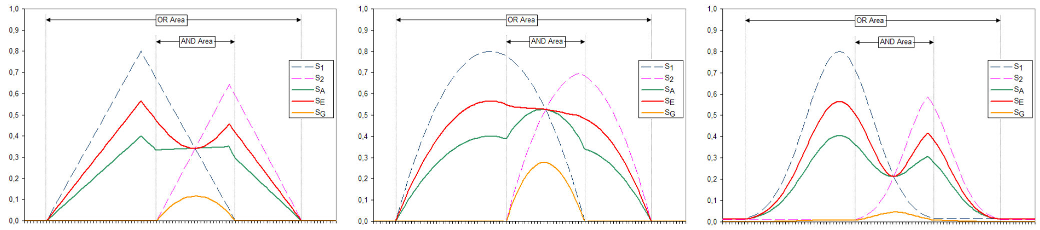

(a) (b) (c)

Figure 3: Depiction of fusion of similarities: (a) after linear mapping; (b) after quadratic mapping; and (c) after Gaussian mapping.

Note that the above definition is a generalization of the z-score normalization and median normalization [12].

A *normalized similarity measure* to target S_f can be derived from D_f as:

a. Linear mapping:

$$S_f = 1 - D_f \ . \tag{2}$$

This is the classic linear distance to similarity transformation [26].

b. Quadratic mapping:

$$S_f = 1 - D_f^2 \ . \tag{3}$$

We introduce quadratic mapping, which favors close to target feature values. Note that D_f^2 behaves like the potential energy of elasticity.

c. Gaussian mapping:

$$S_f = exp(-\alpha D_f^2) \ , \tag{4}$$

where α is the drop-off parameter. We introduce Gaussian mapping, for smoothing out large distance measures. Note that the Gaussian tails can be cut at the cut-off values.

Comments:

a. If the target value is the mean of the feature values and the cut-off is its standard deviation then

$$D_f = \frac{|v_f - \mu_f|}{\sigma_f} \ , \tag{5}$$

and Eq. 1 becomes similar to the z-score normalization of feature values [12].

b. If the target value is the median of the feature values and the cut-off is its median absolute deviation (MAD) then

$$D_f = \frac{|v_f - median_f|}{median\left(|v_f - median_f|\right)} \ , \tag{6}$$

and Eq. 1 becomes similar to the median normalization of feature values [12].

c. $D_f(c_f)$ is a decreasing function of c_f and $S_f(c_f)$ is an increasing function of c_f. As c_f increases, f-axis shrinks and similarity values approach maximum similarity (1.00 or w_f), on the contrary as c_f decreases f-axis dilates and similarity values deviate from maximum similarity (1.00 or w_f).

3.2 Feature similarity fusion

The resultant similarity measure to the target vector in the normalized similarity space describes the way by which the N feature descriptors can be fused together or combined into a resultant feature similarity for each queried landmark class:
a. Sum rule:

$$S_A = \frac{1}{N} \sum_{f=1}^{N} S_f \ , \tag{7}$$

which is the arithmetic mean or the Manhattan (L_1) metric (Fig. 2). Note that if the similarity measure is considered as the probability that the sample point is similar to the target, then this metric is equivalent to the *sum rule* for feature fusion [15, 26].
b. Root-mean-square rule:

$$S_E = \frac{1}{\sqrt{N}} \left(\sum_{f=1}^{N} S_f^2 \right)^{\frac{1}{2}} \ , \tag{8}$$

which is the root mean square (rms) of the similarities and actually a Euclidean (L_2) metric in the resultant similarity space. We introduce this novel *rms rule* so that feature similarities to targets can be considered as vectors and added according to vector addition (Fig. 2).
c. Product rule:

$$S_G = \left(\prod_{f=1}^{N} S_f \right)^{\frac{1}{N}} \ , \tag{9}$$

which is the geometric mean metric. Note that if the similarity measure is considered as the probability that the sample point is similar to the target, then this metric is equivalent to the *product rule* for feature fusion [15, 26].
d. Max rule:

$$S_{max} = \max_{f=1}^{N} (S_f) \ , \tag{10}$$

which is the L_∞ metric or *max rule* [15] and favors the feature with maximum similarity. Note that if the similarity measure is considered as a fuzzy variable, then this metric is equivalent to a fuzzy *OR rule* for feature fusion [26].
e. Min rule:

$$S_{min} = \min_{f=1}^{N} (S_f) \ , \tag{11}$$

which is the *min rule* [15] and favors the feature with minimum similarity. Note that if the similarity measure is considered as a fuzzy variable, then this metric is equivalent to a fuzzy *AND rule* for feature fusion [26].

Comments:
a. If linear mapping and arithmetic mean is used, then the overall similarity measure is consistent with the overall distance measure.
$S_A = \frac{1}{N} \sum_{f=1}^{N} S_f$ and $S_f = 1 - D_f$, then

$S_A = \frac{1}{N}\sum_{f=1}^{N}(1-D_f) \Rightarrow S_A = \frac{N}{N} - \frac{1}{N}\sum_{f=1}^{N} D_f \Rightarrow S_A = 1 - D_A$.
b. The S_A resultant similarity (L_1 metric) is equivalent to the normalized projection of the S_E similarity vector (L_2 metric) onto the target similarity vector S_T (Fig. 2) (i.e. it is a normalized inner product metric, or the *cosine similarity measure* [26]. $\frac{\overrightarrow{S_E}}{\sqrt{N}} \cdot \frac{\overrightarrow{S_T}}{\sqrt{N}} = \frac{1}{N}\sum_{f=1}^{N} S_f \cdot 1 = S_A$.

To illustrate the behavior of the proposed distance to similarity mappings and the fusion schemes we depict the various combinations in Fig. 3. For simplicity the fusion of similarity mapping functions is presented in a single dimension.

Comments:
a. Linear mapping raise discontinuities in the superposed similarities. The "smoothest" results are given by the Gaussian mapping.
b. S_G and S_{min} give results in the "AND Area" and S_A, S_E and S_{max} give results in the "OR Area".
c. S_G and S_{min} give almost the same peak, approximately in the middle of the initial peaks of the fused features, having a similar to an "AND operator" behavior. This peak is "smoother" for S_G and "sharper" for S_{min}.
d. S_{max} gives the same peaks as the initial peaks of the fused features, having a similar to an "OR operator" behavior.

3.3 Weighted metrics

With the above metrics each feature contributes equally to the resultant similarity. Extended similarity metrics with weights per feature can also be considered:
a. Sum rule:

$$S_A = \frac{1}{W}\sum_{f=1}^{N} w_f S_f \ , \ W = \sum_{f=1}^{N} w_f \ . \tag{12}$$

b. Root-mean-square rule:

$$S_E = \frac{1}{\sqrt{W}}\left(\sum_{f=1}^{N} w_f S_f\right)^{\frac{1}{2}} \ , \ W = \sum_{f=1}^{N} w_f \ . \tag{13}$$

c. Product rule:

$$S_G = \left(\frac{1}{W}\prod_{f=1}^{N} w_f S_f\right)^{\frac{1}{N}} \ , \ W = \max_{f=1}^{N}(w_f) \ . \tag{14}$$

d. Max rule:

$$S_{max} = \frac{1}{W}\max_{f=1}^{N}(w_f S_f) \ , \ W = \max_{f=1}^{N}(w_f) \ . \tag{15}$$

e. Min rule:

$$S_{min} = \frac{1}{W} \min_{f=1}^{N} (w_f S_f) \ , \ W = \max_{f=1}^{N} (w_f) \ . \tag{16}$$

Comments: The weights w_f act as scaling factors on the feature similarity components, and can take values $[0.0, 1.0]$. They actually correspond to the maximum similarity value a feature can take, which, as a first approximation, is proportional to the reliability of a feature in respect to other features.

4 Similarity mapping and fusion paradigms

To illustrate the characteristics of the proposed distance to similarity mappings and the fusion schemes we apply them for the detection of specific facial anatomical landmarks.
a. The landmark classes are:
1) the Eye Outer Corner (**EOC**)
2) the Eye Inner Corner (**EIC**)
3) the Nose Tip (**NT**)
4) the Mouth Corner (**MC**), and
5) the Chin Tip (**CT**).
b. The descriptors that are used are:
1) the Shape Index (**SI**)
2) the Spin Image (**SS**), and
3) the Edge Response (**ER**).
c. The distance to similarity mappings are:
1) the linear mapping (**L**)
2) the quadratic mapping (**Q**), and
3) the Gaussian mapping (**G**).
d. The fusion schemes are:
1) the sum rule using the arithmetic mean S_A (**L1**)
2) the rms rule using the Euclidean mean S_E (**L2**)
3) the product rule using the geometric mean S_G (**Lg**)
4) the max rule using S_{max} (**Lmax**)
5) the min rule using S_{min} (**Lmin**).

4.1 Landmark Descriptors

To detect landmark points, we have used two 3D local shape descriptors that exploit the 3D geometry-based information of the facial datasets and one 2D local appearance descriptor that exploits the 2D intensity-based information: the *shape index*, the *spin images* and the *edge response*.

A facial scan belongs to a subclass of 3D objects which is a surface S expressed in parametric form with native (u, v) parameterization which also incorporates texture data. This parameterization allows to map 3D information onto 2D space and vice-versa, thus the 3D and 2D information can be cross-referenced [19, 20].

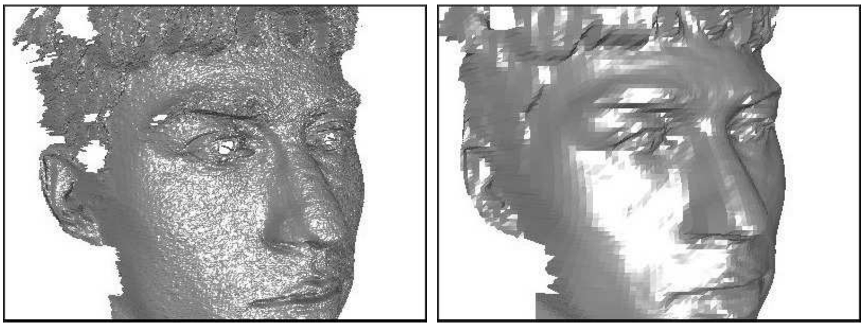

(a) (b)

Figure 4: Example of a facial scan (a) before and (b) after preprocessing.

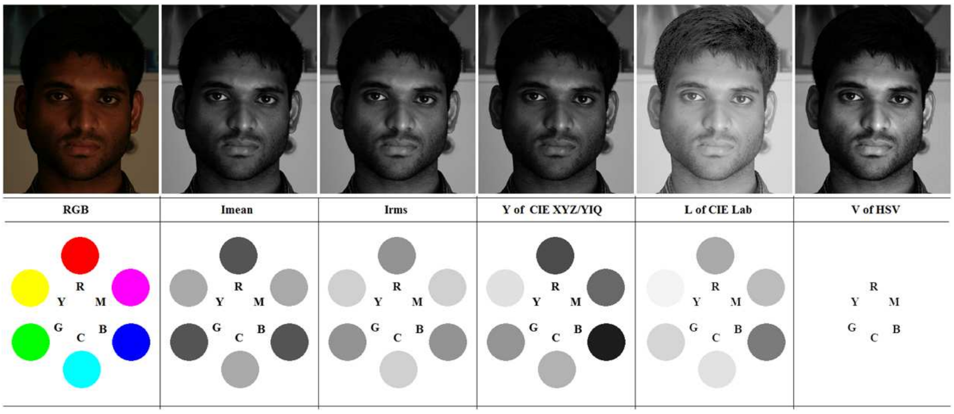

Figure 5: Depiction of various RGB to B/W transformations of images.

Since differential geometry is used for describing the local behavior of surfaces (such as surface curvature and surface normals), we assume that the surface S can be adequately modeled as being at least piecewise smooth. Therefore, to eliminate sensor-specific problems, such as white noise, spikes and holes (especially in areas like the eyebrows and the eyes), certain preprocessing algorithms (median cut, hole filling, smoothing, and subsampling) operate directly on the range data before the conversion to polygonal data [14, 19] (Fig. 4).

Also, since the texture images are in (R,G,B) space we need to convert them into B/W intensity images, appropriate for the application of intensity differential operators. For this purpose we used the L component of the CIE Lab color model [17], since it fixes to some extent the shadings due to illumination conditions, and gives more equalized intensity histograms (Fig. 5).

4.1.1 The Shape Index Descriptor

The *Shape Index* [7, 16] is a continuous mapping of principal curvature values (k_{max}, k_{min}) of a 3D object point $\mathbf{p}$ into the interval [0,1], and is computed as:

$$SI(\mathbf{p}) = \frac{1}{2} - \frac{1}{\pi} tan^{-1} \frac{k_{max}(\mathbf{p}) + k_{min}(\mathbf{p})}{k_{max}(\mathbf{p}) - k_{min}(\mathbf{p})} \ . \tag{17}$$

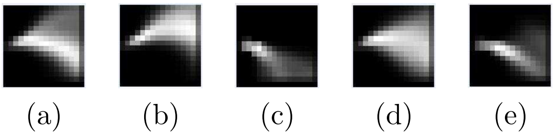

Figure 6: Depiction of spin image templates: (a) eye outer corner (EOC); (b) eye inner corner (EIC); (c) nose tip (NT); (d) mouth corner (MC); and (e) chin tip (CT).

The shape index captures the intuitive notion of "local" shape of a surface. Five well-known shape types and their shape index values are: Cup = 0.0, Rut = 0.25, Saddle = 0.5, Ridge = 0.75, and Cap = 1.0.

Shape index is computed from the principal curvature values of the surface spanned by the nearest neighbors of each vertex, a region of 5.5 *mm* radius on average.

4.1.2 The Spin Image Descriptor

A *Spin Image* [13] encodes the coordinates of points on the surface of a 3D object with respect to a so-called *oriented point* $(\mathbf{p}, \mathbf{n})$, where $\mathbf{n}$ is the normal vector at a point $\mathbf{p}$ of a 3D object surface. A spin image at an oriented point $(\mathbf{p}, \mathbf{n})$ is a 2D grid accumulator of 3D points, as the grid is rotated around $\mathbf{n}$ by 360°. Thus, a spin image is a descriptor of the global or local shape of the object, invariant under rigid transformations. Locality is expressed by the size of the spin image grid and the size of the grid cells (bins). For the purpose of representing facial features on 3D facial datasets, it was experimentally determined that a 16×16 spin image grid with 2 *mm* bin size should be used. This represents the local shape of the neighborhood of each landmark, spanned by a cylinder of 3.2 *cm* height and 3.2 *cm* radius.

The similarity measure between a spin image P and a spin image template Q is expressed by the normalized linear correlation coefficient [13]:

$$SS(P, Q) = \frac{N \sum p_i q_i - \sum p_i \sum q_i}{\sqrt{\left[N \sum p_i^2 - (\sum p_i)^2\right] \left[N \sum q_i^2 - (\sum q_i)^2\right]}} \, , \tag{18}$$

where p_i, q_i denote each of the N elements of spin images P and Q, respectively.

4.1.3 The Edge Response Descriptor

The *Edge Response* is based on the well known Harris corner and edge detector [9]. A response function $ER(\mathbf{p})$ encodes the intensity gradient of a point $\mathbf{p}$ on an image:

$$ER(\mathbf{p}) = I_x^2(\mathbf{p}) + I_y^2(\mathbf{p}) \, , \tag{19}$$

where $I_x = \frac{\partial I}{\partial x}$ and $I_y = \frac{\partial I}{\partial y}$ denote the partial derivatives of the intensity image I in x and y respectively. $ER(\mathbf{p})$ is high in edge regions and close to zero in flat regions. In our implementation of calculating $ER(\mathbf{p})$, Sobel masks are convolved with the intensity image for the calculation of I_x and I_y [8], which are subsequently filtered by a Gaussian mask (7×7 pixels and $\sigma = 1.0$).

Table 1: Target (t) and cut-off (c) values of the landmark descriptors for each landmark class

	EOC		EIC		NT		MC		CT	
	t	c	t	c	t	c	t	c	t	c
SI	0.32	0.53	0.12	0.60	1.00	0.40	0.09	0.68	0.96	0.70
SS	1.00	0.48	1.00	0.80	1.00	0.75	1.00	0.72	1.00	0.56
ER	0.20	0.72	0.16	0.62	0.10	0.40	0.22	0.70	0.02	0.17

Table 2: Correlation coefficients between landmark descriptors for each landmark class

	EOC	EIC	NT	MC	CT
Raw values					
SI / SS	0.0358	−0.1242	0.3202	−0.1823	0.1925
SI / ER	0.1458	0.0024	−0.0895	0.0000	0.0001
SS / ER	−0.0377	−0.1358	−0.1794	−0.2481	−0.0075
Linear mapping similarity values (L)					
SI / SS	0.1781	0.1806	0.3202	0.2669	0.2290
SI / ER	0.1665	0.0360	0.0638	0.1354	−0.0265
SS / ER	0.1080	0.0813	0.1002	0.1991	−0.0013
Quadratic mapping similarity values (Q)					
SI / SS	0.2095	0.1965	0.3098	0.2366	0.5241
SI / ER	0.1968	−0.0101	0.0572	0.0543	−0.0222
SS / ER	0.1184	0.0907	0.0370	0.1849	−0.0093
Gaussian mapping similarity values (G)					
SI / SS	0.2084	0.1921	0.3170	0.2508	0.3459
SI / ER	0.2023	0.0003	0.0524	0.0882	−0.0241
SS / ER	0.1205	0.0989	0.0614	0.2052	−0.0018

4.2 Training of the descriptors

To train the landmark descriptors we used 300 frontal facial datasets of different subjects, manually annotated at the specific landmark positions. These datasets come from FRGC v2 database [22, 21] and contain subjects with varying expressions and illumination conditions. The available 3D scans were used to train the shape index and spin image descriptors and the corresponding 2D texture images to train the edge response descriptor. The exact datasets that were used from the source databases for training (DB_TRAIN) can be found from the landmark annotation files available through our website [28].

The pdf of the shape index values (SI) and edge response values (ER) for each landmark class were computed and used for the estimation of the shape index and edge response target and cut-off values. We computed spin image templates for each landmark class. Spin image templates represent the mean spin image associated with the five classes of landmarks (Fig. 6). The pdfs of the similarity values (SS) between the pre-computed spin image templates and the spin images of each landmark class, were computed for the estimation of the cut-off values. The spin image target values

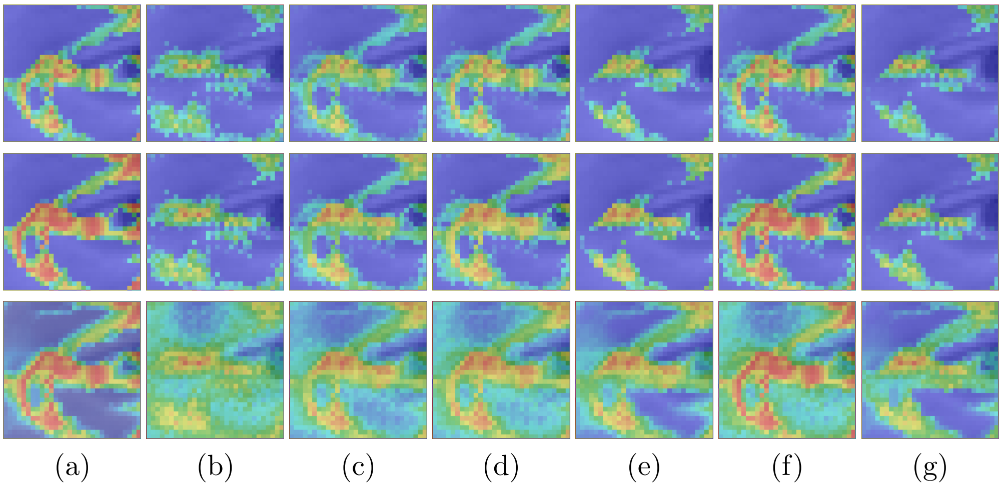

Figure 7: Depiction of the 2D similarity maps of the Eye Outer Corner (EOC) for the various distance to similarity mappings and the various fusion methods: (blue) low similarity values (0.0); (green) medium similarity values (0.5); and (red) high similarity values (1.0). **(top)** L mapping; **(middle)** Q mapping; and **(bottom)** G mapping. (a) SI similarity; (b) SS similarity; (c) L1 fusion; (d) L2 fusion; (e) Lg fusion; (e) Lmax fusion; and (f) Lmin fusion.

are set to the maximum similarity (1.00).

The estimated target and cut-off values for each descriptor (SI, SS, ER) and for each landmark class (EOC, EIC, NT, MC, CT) are presented in Table 1, and the correlation coefficients between the landmark descriptors for each landmark class are presented in Table 2. Note that the introduction of distance to similarity mappings improves the correlation coefficients in comparison to the raw values.

5 Experimental Results

5.1 Test Databases

For the purposes of this evaluation, we used two databases:
(i) a database with 975 frontal facial datasets obtained from 149 different subjects, selected from the FRGC v2 database [22, 21], including subjects with varying degrees of expressions (45.44% "neutral", 36.41% "mild" and 18.15% "extreme"), acquired under varying illumination conditions. This database will henceforth be referred as **DB00F**.
(ii) a composite database with the datasets of 39 common subjects found in the FRGC v2 database and in the UND Ear database [29]. This database consists of 117 (3x39) facial scans having three poses, frontal (39 scans) and 45 degrees left (39 scans) and right (39 scans), and will henceforth be referred as **DB00F45RL**.

5.2 Performance Evaluation

The evaluation of the performance of the proposed distance to similarity mappings and fusion schemes for landmark detection is not a straight-forward task, since there

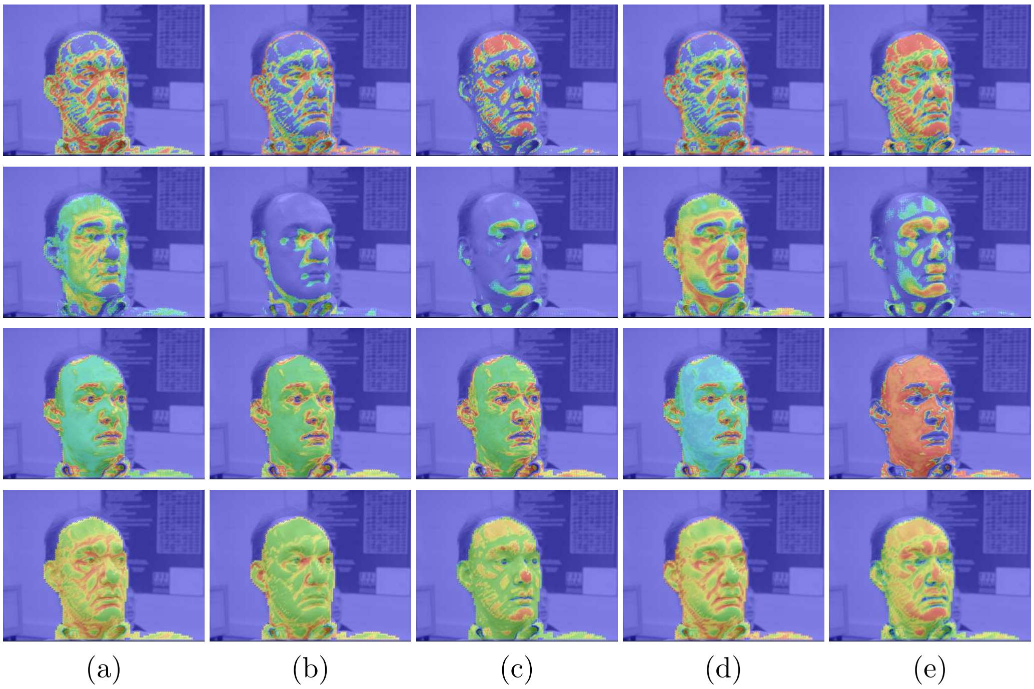

Figure 8: Depiction of feature similarity maps with Q−L2 fusion: (blue) low similarity values (0.0); (green) medium similarity values (0.5); and (red) high similarity values (1.0). (**1$^{\text{st}}$ row**) SI similarity; (**2$^{\text{nd}}$ row**) SS similarity; (**3$^{\text{rd}}$ row**) ER similarity; and (**4$^{\text{th}}$ row**) Q−L2 resultant similarity. (**a**) eye outer corner; (**b**) eye inner corner; (**c**) nose tip; (**d**) mouth corner; and (**e**) chin tip.

are many factors that characterize performance. As already stated, fusion techniques are expected to improve system's *accuracy*, *efficiency* and *robustness*. An equally important characteristic of a fusion scheme is that of *monotonicity*, i.e., the addition of a new feature descriptor should improve prior results.

Thus, we evaluate performance according to these four characteristics. *Accuracy* is evaluated according to the distance between the selected optimal landmark and the manually annotated landmark, which is considered as ground-truth. The selected optimal landmark is the 1^{st} rank candidate landmark for each landmark class (i.e., the candidate landmark which has the maximum resultant similarity score). *Efficiency* is evaluated according to the reduction of the likelihood area of a landmark class (see Fig. 8 high similarity areas). The likelihood area of a landmark class is very important since its reduction means that fewer candidate landmarks have to be retained and fed to the "selection level". *Robustness* is evaluated by the use of testing datasets which contain subjects acquired under large yaw rotations, varying expressions and different illumination conditions, and also by the use of five different landmark classes. *Monotonicity* is evaluated according to the accuracy improvement between the use of individual descriptors, the fusion of the two richest descriptors, the shape index (SI) and the spin image (SS), and the fusion with the addition of a third poorer descriptor, the edge response (ER).

A qualitative performance evaluation of the proposed fusion schemes according

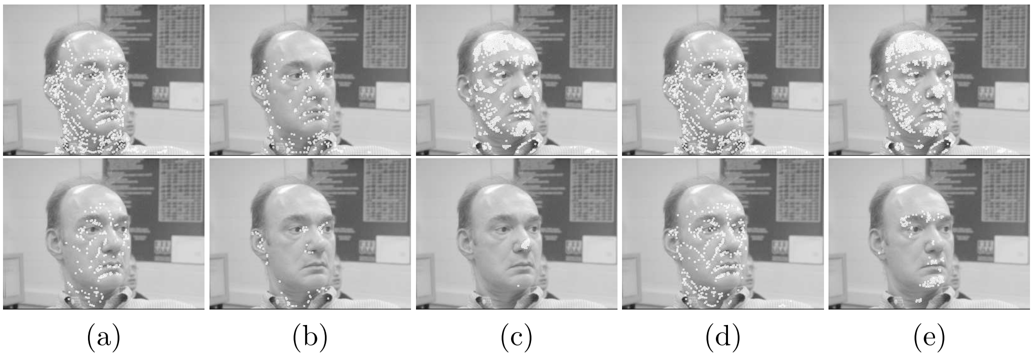

Figure 9: Depiction of detected candidate landmarks on texture image: **(top)** SI and SS fusion; and **(bottom)** SI, SS and ER fusion. (a) eye outer corner; (b) eye inner corner; (c) nose tip; (d) mouth corner; and (e) chin tip.

Table 3: Qualitative evaluation of proposed fusion schemes

	Accuracy	Efficiency	Robustness	Monotonicity
L−L1	Fair	**High**	Fair	Fair
L−L2	Fair	Low	Fair	Fair
L−Lg	**High**	Fair	Fair	Fair
Q−L1	**High**	**High**	Fair	Fair
Q−L2	**High**	**High**	**High**	**High**
Q−Lg	**High**	Fair	Fair	Fair
G−L1	**High**	**High**	**High**	**High**
G−L2	**High**	**High**	Fair	Fair
G−Lg	**High**	Fair	Fair	Fair
L−Lmax	Low	Low	Low	Low
Q−Lmax	Low	Low	Low	Low
G−Lmax	Low	Low	Low	Low
L−Lmin	Unreliable	Fair	Fair	Low
Q−Lmin	Unreliable	Fair	Fair	Low
G−Lmin	Unreliable	Fair	Fair	Low

to the aforementioned characteristics is presented in Table 3. Detailed landmark localization error analysis is presented in Tables 4 and 5.

Our experimental findings are similar to those of [11], which are summarized in the following:
i) There is no single combination rule that scores best for all cases.
ii) Combining does not necessarily lead to improved performance.
iii) There are cases where none of the combining rules does better than the best individual detector.

Despite these general findings a more detailed examination of the results shows that there are some fusion schemes that perform better in most cases and can be adopted, and others that perform quite poorly and should be avoided.

Our results show that, in general, the Quadratic (Q) and Gaussian (G) mappings behave better than the Linear (L) mapping. For the Linear mapping the product rule (Lg) behaves better than other rules. For the Quadratic mapping the rms rule (L2) behaves better than other rules. For the Gaussian mapping the sum rule (L1) behaves better than other rules. Quadratic and Gaussian mappings have almost the same performance.

The introduction of the Edge Response (ER) descriptor improves the results for the EOC, EIC and MC landmarks, but degrades the results for NT and CT. Note that, although ER is a poor descriptor, the improvement in accuracy is more dramatic in MC and EOC where the ER descriptor is more correlated with the SI and SS descriptors. Also note that the decline in accuracy is more dramatic in NT and CT where the ER descriptor is uncorrelated with the SI and SS descriptors (Table 2).

Accuracy improvement is more dramatic when the information fused is correlated. In correlated features the performance of one descriptor predicts to some extent the performance of the other and strengthens the results. On the other hand highly uncorrelated features have similarity peaks that do not coincide and degrade the results. Efficiency improvement is achieved by excluding obvious non-matches, reducing the number of candidate landmarks, for each landmark class. Fusion, also, reduces system sensitivity to sample-specific, poor-quality or erroneous descriptors.

We can thus deduce that the best performance in terms of accuracy is exhibited by the Q-L2 and G-L1 fusion schemes, with the Q-L2 exhibiting a slight better performance than the G-L1 in landmarks' likelihood area reduction. Q-L2 and G-L1 also exhibit high robustness in yaw, expression and illumination variations, and strong monotonicity.

6 Conclusion

A novel generalized framework of fusion methods and their application to landmark detection has been presented. The proposed fusion scheme acts after the "feature extraction level", transforms features to similarities and then combines them to generate a resultant feature similarity, which is considered as the matching score used at the "matching level" for the detection of the queried landmarks. The proposed feature fusion scheme is easily extendable to new feature-components in feature space, offers significant dimensionality reduction and works equally well for features extracted from 3D or 2D facial data.

For the proposed fusion scheme different distance to similarity mappings (linear, quadratic and Gaussian) and different fusion rules (sum rule, rms rule, product rule, max rule and min rule) have been evaluated according to *accuracy*, *efficiency*, *robustness* and *monotonicity*. The results indicate that the quadratic distance to similarity mapping in conjunction with the rms rule for fusion (Q-L2) exhibits the best performance.

Acknowledgment

This research has been co-financed by the European Union (European Social Fund - ESF) and Greek national funds through the Operational Program "Education and Lifelong Learning" of the National Strategic Reference Framework (NSRF) - Research Funding Program: Heracleitus II. Investing in knowledge society through the European Social Fund.

European Union
European Social Fund

OPERATIONAL PROGRAMME
EDUCATION AND LIFELONG LEARNING
investing in knowledge society
MINISTRY OF EDUCATION & RELIGIOUS AFFAIRS, CULTURE & SPORTS
MANAGING AUTHORITY

NSRF
2007-2013
programme for development
EUROPEAN SOCIAL FUND

Co-financed by Greece and the European Union

References

[1] C. Boehnen and T. Russ, *A fast multi-modal approach to facial feature detection*, Proc. 7th IEEE Workshop on Applications in Computer Vision, vol. 1, Jan. 5-7 2005, pp. 135–142.

[2] E. Bossè, A. Guitouni, and P. Valin, *An essay to characterise information fusion systems*, Proc. 9th International Conference on Information Fusion (Florence, Italy), Jul. 10-13 2006, pp. 1–7.

[3] T. Cootes and C. Taylor, *Statistical models of appearance for computer vision*, Tech. report, University of Manchester, Oct. 2001.

[4] T. Cootes, K. Walker, and C. Taylor, *View-based active appearance models*, Proc. IEEE International Conference on Automatic Face and Gesture Recognition (Grenoble, France), Mar. 26-30 2002, pp. 227–232.

[5] T.F. Cootes, C.J. Taylor, D.H. Cooper, and J. Graham, *Active shape models - their training and application*, Computer Vision and Image Understanding **61** (1995), no. 1, 38–59.

[6] D. Cristinacce and T. Cootes, *Automatic feature localization with constrained local models*, Pattern Recognition **41** (2008), no. 10, 3054–3067.

[7] C. Dorai and A. K. Jain, *COSMOS - a representation scheme for 3D free-form objects*, IEEE Transactions on Pattern Analysis and Machine Intelligence **19** (1997), no. 10, 1115–1130.

[8] R. C. Gonzalez and R. E. Woods, *Digital image processing*, 2nd ed., Prentice-Hall, 2002.

[9] C. Harris and M. Stephens, *A combined corner and edge detector*, Proc. 4th Alvey Vision Conference, 1988, pp. 147–151.

[10] S. Jahanbin, H. Choi, and A.C. Bovik, *Passive multimodal 2-D+3-D face recognition using gabor features and landmark distances*, IEEE Transactions on Information Forensics and Security **6** (2011), no. 4, 1287–1304.

[11] A. Jain, R. Duin, and J. Mao, *Statistical pattern recognition: A review*, IEEE Transactions on Pattern Analysis and Machine Inteligence **22** (2000), no. 1, 4–37.

[12] A. Jain, K. Nandakumar, and A. Ross, *Score normalization in multimodal biometric systems*, Pattern Recognition **38** (2005), no. 12, 2270–2285.

[13] A. E. Johnson, *Spin Images: A Representation for 3-D Surface Matching*, Ph.D. thesis, Robotics Institute, Carnegie Mellon University, Pittsburgh, PA, Aug. 1997.

[14] I.A. Kakadiaris, G. Passalis, G. Toderici, M.N. Murtuza, Y. Lu, N. Karampatziakis, and T. Theoharis, *Three-dimensional face recognition in the presence of facial expressions: An annotated deformable model approach*, IEEE Transactions on Pattern Analysis and Machine Intelligence **29** (2007), no. 4, 640–649.

[15] J. Kittler, M. Hatef, R. Duin, and J. Matas, *On combining classifiers*, IEEE Transactions on Pattern Analysis an Machine Inteligence **20** (1998), no. 3, 226–239.

[16] J. Koenderink and A. van Doorn, *Surface shape and curvature scales*, Image and Vision Computing **10** (1992), 557–565.

[17] Z-N. Li and M. S. Drew, *Fundamentals of multimedia*, Pearson Education, 2004.

[18] X. Lu and A. Jain, *Multimodal facial feature extraction for automatic 3D face recognition*, Tech. Report MSU-CSE-05-22, Michigan State University, Oct. 2005.

[19] G. Passalis, P. Perakis, T. Theoharis, and I.A. Kakadiaris, *Using facial symmetry to handle pose variations in real-world 3D face recognition*, IEEE Transactions on Pattern Analysis and Machine Intelligence **33** (2011), no. 10, 1938–1951.

[20] P. Perakis, T. Theoharis, G. Passalis, and I.A. Kakadiaris, *Automatic 3D facial region retrieval from multi-pose facial datasets*, Proc. Eurographics Workshop on 3D Object Retrieval (Munich, Germany), Mar. 30 - Apr. 3 2009, pp. 37–44.

[21] P. Phillips, T. Scruggs, A. O'Toole, P. Flynn, K. Bowyer, C. Schott, and M. Sharpe, *FRVT 2006 and ICE 2006 large-scale experimental results*, IEEE Transactions on Pattern Analysis and Machine Intelligence **32** (2010), 831–846.

[22] P.J. Phillips, P.J. Flynn, T. Scruggs, K.W. Bowyer, J. Chang, K. Hoffman, J. Marques, J. Min, and W. Worek, *Overview of the Face Recognition Grand Challenge*, Proc. IEEE Conference on Computer Vision and Pattern Recognition (San Diego, CA), 2005, pp. 947–954.

[23] A. Ross and R. Govindarajan, *Feature level fusion using hand and face biometrics*, Proc. SPIE Conference on Biometric Technology for Human Identification II (Orlando, USA), Mar. 2005, pp. 196–204.

[24] A. Ross and A. Jain, *Information fusion in biometrics*, Pattern Recognition Letters **24** (2003), no. 13, 2115–2125.

[25] R. Snelick, U. Uludag, A. Mink, M. Indovina, and A. Jain, *Large-scale evaluation of multimodal biometric authentication using state-of-the-art systems*, IEEE Transactions on Pattern Analysis an Machine Inteligence **27** (2005), no. 3, 450–455.

[26] S. Theodoridis and K. Koutroumbas, *Pattern recognition*, 3^{rd} ed., Academic Press, 2006.

[27] T. Theoharis, G. Passalis, G. Toderici, and I.A. Kakadiaris, *Unified 3D face and ear recognition using wavelets on geometry images*, Pattern Recognition **41** (2008), no. 3, 796–804.

[28] UH-CBL, *Facial Landmarks Annotation Files*, http://www.cbl.uh.edu/URxD/annotations/facial-landmarks.zip, 2012, ver. 3.

[29] UND, *University of Notre Dame Biometrics Data Sets*, http://www.nd.edu/∼cvrl/CVRL/Data_Sets.html, 2012.

[30] L. Xu, A. Krzyzak, and C. Suen, *Methods for combining multiple classifiers and their applications to handwriting recognition*, IEEE Transactions on System, Man, and Cybernetics **22** (1992), no. 3, 418–435.

Table 4: Landmark localization distance-error (*mm*) results of Shape Index (SI), Spin Image (SS) and Edge Response (ER) fusion, in **DB00F** and **DB00F45RL**

DB00F − Landmark localization error (*mm*)						
	EOC	EIC	NT	MC	CT	Mean
SI	11.72	7.71	14.66	**5.98**	10.81	10.18
SS	**7.31**	**4.42**	**3.84**	8.47	**7.56**	**6.32**
ER	12.26	13.05	10.54	9.27	11.74	11.37
L−L1	6.40	4.60	4.12	**4.82**	**7.16**	5.42
L−L2	6.72	4.74	4.19	4.78	7.24	5.53
L−Lg	**6.31**	**4.52**	**4.08**	4.85	7.23	**5.40**
Q−L1	6.21	4.15	3.97	4.90	7.31	5.31
Q−L2	**6.19**	**4.14**	3.97	**4.87**	**7.28**	**5.29**
Q−Lg	6.20	4.15	**3.95**	4.92	7.29	5.30
G−L1	6.19	**4.14**	**3.97**	**4.86**	**7.28**	**5.29**
G−L2	**6.16**	4.15	3.98	4.89	**7.28**	**5.29**
G−Lg	6.21	4.15	**3.97**	4.90	7.31	5.31
L−Lmax	11.93	11.57	14.66	8.45	11.63	11.65
Q−Lmax	12.17	11.50	14.69	8.49	12.05	11.78
G−Lmax	12.17	11.50	14.69	8.49	12.05	11.78
L−Lmin	7.21	3.97	3.88	5.23	8.41	5.74
Q−Lmin	7.21	3.97	3.88	5.23	8.41	5.74
G−Lmin	7.21	3.97	3.88	5.23	8.41	5.47

DB00F45RL − Landmark localization error (*mm*)						
	EOC	EIC	NT	MC	CT	Mean
SI	10.99	7.20	12.51	**4.68**	11.26	9.33
SS	**9.16**	**4.83**	**3.68**	7.03	**7.24**	**6.39**
ER	11.31	12.10	11.79	9.16	12.29	11.33
L−L1	**6.97**	**4.94**	4.40	**4.09**	**7.56**	**5.59**
L−L2	7.22	5.11	4.88	**4.09**	7.57	5.77
L−Lg	6.98	4.95	**4.20**	4.14	7.69	**5.59**
Q−L1	6.89	**4.59**	3.82	**3.83**	7.80	5.39
Q−L2	6.80	**4.59**	3.82	**3.83**	**7.73**	**5.35**
Q−Lg	**6.77**	**4.59**	**3.80**	**3.83**	7.79	5.36
G−L1	**6.80**	**4.59**	**3.82**	**3.83**	**7.73**	**5.35**
G−L2	6.85	4.64	3.84	**3.83**	**7.73**	5.38
G−Lg	6.89	**4.59**	**3.82**	**3.83**	7.80	5.39
L−Lmax	11.89	10.86	12.51	7.91	11.96	11.03
Q−Lmax	12.01	10.79	12.51	7.91	12.44	11.13
G−Lmax	12.01	10.79	12.51	7.91	12.44	11.13
L−Lmin	8.53	4.64	3.53	4.42	7.88	5.80
Q−Lmin	8.53	4.64	3.53	4.42	7.88	5.80
G−Lmin	8.53	4.64	3.53	4.42	7.88	5.80

Table 5: Landmark localization distance-error (mm) results of Shape Index (SI) and Spin Image (SS) fusion, in **DB00F** and **DB00F45RL**

DB00F – Landmark localization error (mm)						
	EOC	EIC	NT	MC	CT	Mean
SI	11.72	7.71	14.66	**5.98**	10.81	10.18
SS	**7.31**	**4.42**	**3.84**	8.47	**7.56**	**6.32**
L–L1	7.58	4.81	**3.85**	5.85	7.30	5.88
L–L2	7.70	4.84	**3.85**	5.81	**7.16**	**5.87**
L–Lg	**7.54**	**4.80**	**3.85**	**5.80**	7.38	**5.87**
Q–L1	7.54	4.73	**3.84**	**5.84**	**7.28**	5.85
Q–L2	**7.52**	**4.72**	3.85	**5.84**	**7.28**	**5.84**
Q–Lg	7.53	4.73	3.85	5.87	7.29	5.85
G–L1	**7.52**	**4.72**	3.85	**5.84**	**7.28**	**5.84**
G–L2	7.53	**4.72**	**3.84**	**5.84**	**7.28**	**5.84**
G–Lg	7.54	4.73	**3.84**	**5.84**	**7.28**	5.85
L–Lmax	11.72	7.71	14.66	6.06	10.81	10.19
Q–Lmax	11.72	7.72	14.66	6.06	10.81	10.19
G–Lmax	11.72	7.72	14.66	6.06	10.81	11.78
L–Lmin	7.34	4.61	3.84	5.91	7.39	5.82
Q–Lmin	7.34	4.61	3.84	5.91	7.39	5.82
G–Lmin	7.34	4.61	3.84	5.91	7.39	5.82

DB00F45RL – Landmark localization error (mm)						
	EOC	EIC	NT	MC	CT	Mean
SI	10.99	7.20	12.51	**4.68**	11.26	9.33
SS	**9.16**	**4.83**	**3.68**	7.03	**7.24**	**6.39**
L–L1	8.82	5.11	**3.67**	5.04	7.38	6.00
L–L2	8.80	5.06	**3.67**	5.03	7.53	6.02
L–Lg	**8.53**	**5.05**	**3.67**	**4.99**	**7.35**	**5.92**
Q–L1	8.39	4.98	**3.62**	**4.72**	**7.53**	5.85
Q–L2	**8.33**	**4.97**	**3.62**	**4.72**	**7.53**	**5.83**
Q–Lg	8.39	**4.97**	**3.62**	**4.72**	7.54	5.85
G–L1	**8.33**	**4.97**	**3.62**	**4.72**	**7.53**	**5.83**
G–L2	8.34	**4.97**	3.67	**4.72**	**7.53**	5.85
G–Lg	8.39	4.98	**3.62**	**4.72**	**7.53**	5.85
L–Lmax	11.00	7.23	12.51	4.68	11.26	9.34
Q–Lmax	10.99	7.20	12.51	4.68	11.26	9.33
G–Lmax	10.99	7.20	12.51	4.68	11.26	9.33
L–Lmin	8.53	4.64	3.53	4.42	7.88	5.80
Q–Lmin	9.20	4.88	3.51	5.03	7.27	5.98
G–Lmin	9.20	4.88	3.51	5.03	7.27	5.98